Electromagnetic Forces in Three-Phase Rigid Busbars with Rectangular Cross-Sections

D.P. Labridis, Member, IEEE P.S. Dokopoulos, Member, IEEE

Power Systems Laboratory
Department of Electrical and Computer Engineering
Aristotle University of Thessaloniki
Thessaloniki, GR-54006 Greece

Abstract **- A three-phase busbar arrangement with straight rigid conductors carrying short-circuit currents is investigated. Calculations are made assuming steady-state ac current with a peak value equal to the peak value of the short-circuit current. This assumption is used in the related IEC Standards 865/92. In this paper, the electromagnetic forces and current densities are calculated by solving the electromagnetic field diffusion equation numerically, using finite elements. The results are compared with results calculated according to the IEC Standards 865/86, as well as with the corresponding technical revision IEC 865/92. The comparison involves arrangements with rectangular cross-sections, as used in ac indoor installations of medium and low voltage. The forces calculated, especially in cases of multiple sub-conductors per main conductor, were greater than those calculated according to the above Standards. In older Standards this difference is up to fifty per cent, while in the revision this difference is smaller. The differences are probably due to proximity effects.**

I. Introduction

Short-circuit currents may exert hazardous forces on busbars, especially in compact indoor installations where distances are relatively small. Therefore a careful consideration of electromagnetic forces and their effects is needed in order to avoid excessive stresses applied on the conductors and bending moments applied on the supporting insulators. Effects of short-circuit currents are analysed in Standards IEC 865:1986 [1] and in a similar way in DIN VDE 0103:04.88 [2]. They cover installations with voltages up to 72.5 kV and frequencies up to 500 Hz. In the corresponding recent technical revisions IEC 865:1992 [8] and DIN/VDE 0103:06.92 [9], the voltage of the systems covered is up to and including 420 kV. The Standards are based on relations for the maximum force presented by Lehmann in [3]. These relations were established on the well-known formula of force acting on filamentary conductors, by making two assumptions. The first assumption is the introduction of the *effective conductor central distance*, a distance that has been introduced in order to take into account the force dependence on the geometrical configuration and the profile of the conductors and computed for DC current only. The second assumption is that the sub-conductors, in arrangements with multiple conductors per main conductor, are assumed to carry the short-circuit current evenly distributed among them. However, due to the proximity effect, the current may differ among sub-conductors. A way to obtain more accurate results is to solve the electromagnetic diffusion equation, which gives the entire information for the field, the current and the force distributions.

Therefore, it seems reasonable to compare results as proposed by Standards [1]-[2] and by their revisions [8]-[9], with calculations obtained from the solution of the electromagnetic field diffusion equation using the finite element method (FEM). In this paper a computation based on finite elements is presented for arrangements of straight three-phase busbars, as used in medium and low voltage substations. Each main conductor consists in generally of up to four rigid sub-conductors, each sub-conductor having a rectangular cross-section. A steady-state three-phase symmetrical current is applied. The geometry of the bus arrangement is taken into account and the current flowing in every sub-conductor is computed from the solution of the electromagnetic field.

95 SM 358-2 PWRD A paper recommended and approved by the IEEE Substations Committee of the IEEE Power Engineering Society for presentation at the 1995 IEEE/PES Summer Meeting, July 23-27, 1995, Portland, OR. Manuscript submitted December 29, 1994; made avaiable for printing April 27, 1995.

II. Computation of Short-Circuit Forces

A. Assumptions

The conventional arrangement of conductors, as shown in Fig. 1 - in parallel and in a single plane - is taken as a basis for the calculations. It is assumed that

- the fault examined is a three-phase symmetrical short-circuit, because it causes the greatest dynamic stress [5];
- the centre-line distance between busbars is much smaller than the conductor length, so that the busbars can be regarded as being of infinite length;
- the permeability is constant, since copper or aluminium bars are used in installations;
- a steady state, balanced three-phase system is applied to the three-phase busbars, with a crest value equal to the crest value of the short-circuit current.

These assumptions have also been used in the related Standards. The balanced three-phase system may be calculated as follows:

The factor κ, that is the ratio of the largest possible asymmetric value of the short-circuit current to the largest symmetric value of the short-circuit current is given by [6]

$$\kappa \approx 1.02 + 0.98 e^{-3R/X} \tag{1a}$$

and the peak short-circuit current is assigned a value

$$i_{p3} = \kappa \sqrt{2}\, I_{k3} \tag{1b}$$

Using the last assumption and (1b), the three-phase currents applied are in phasor form

$$i_a = \frac{I_{p3}}{\sqrt{2}}, \quad i_b = \frac{I_{p3}}{\sqrt{2}} e^{-j2\pi/3}, \quad i_c = \frac{I_{p3}}{\sqrt{2}} e^{-j4\pi/3} \tag{1c}$$

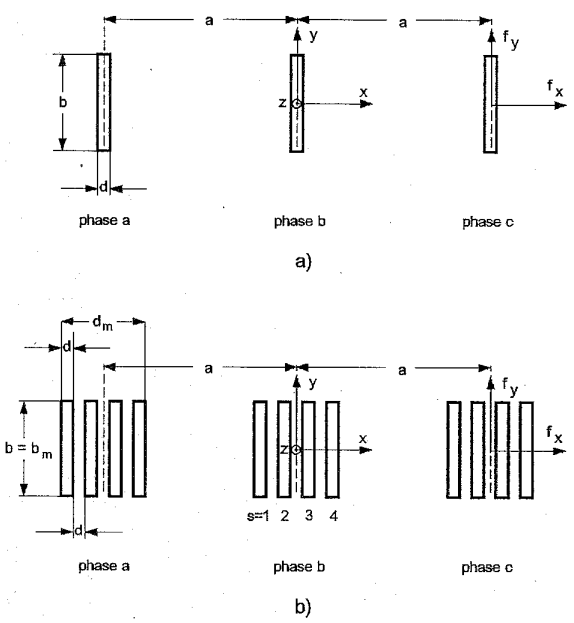

Fig. 1. Cross-section of rigid busbars with:
a) one sub-conductor per main conductor;
b) four sub-conductors per main conductor.

In the above model, steady-state currents have been considered. It would be of interest to extent the present paper to transient currents as well.

B. Field Equations

If the busbar cross-section shown in Fig. 1a-b lies on the *x-y* plane, the linear two-dimensional electromagnetic diffusion problem for the *z*-direction components of the **magnetic vector potential** (MVP) vector A_Z and of the total current density vector J_Z is described [7] by the system of equations

$$\frac{1}{\mu_0 \mu_r}\left[\frac{\partial^2 A_Z}{\partial x^2}+\frac{\partial^2 A_Z}{\partial y^2}\right]-j\omega\sigma A_Z + J_{sz} = 0$$
$$-j\omega\sigma A_Z + J_{sz} = J_Z \qquad (2a)$$

where the *z*-direction component of the total current density J_Z is defined by the integral

$$\iint_{S_i} J_Z ds = I_i \quad , i = a, b, c \qquad (2b)$$

The finite element formulation of equations (2a-b) follows the procedure described in [4] and leads to a similar matrix equation, that is solved using the Crout variation of Gauss elimination. From the solution of this system, the values of the MVP in every node of the discretization domain as well as the unknown source current densities in each busbar are calculated. Consequently, the eddy current density J^e_{ez} of element *e* is obtained from the relation [7]

$$J^e_{ez}(x,y) = -j\omega\sigma A^e_z(x,y) \qquad (3a)$$

and the total element current density J^e_z will be the sum of the phase-*i* busbar source current density $J_{sz\,i}$ and of the element eddy current density J^e_{ez} given by (3a), i.e.

$$J^e_z(x,y) = J^e_{ez}(x,y) + J_{sz\,i} \qquad (3b)$$

Integration of (3b) over a sub-conductor cross-section will give the total current flowing through this sub-conductor.

C. Force Computation

In order to compute the forces acting on every sub-conductor, the flux density in element *e* must be calculated from the MVP element distribution using the relations

$$B^e_x = \frac{\partial A^e_z}{\partial y}$$
$$B^e_y = -\frac{\partial A^e_z}{\partial x} \qquad (4)$$

If the interpolation functions chosen in the finite element formulation are linear polynomial of x and y, then the flux density will be constant on the cross section of every finite element. This simplifies the elementary computations that concern quantities deriving as first derivatives without introducing any error, providing that the finite elements are small enough in order to follow the possible step discontinuities.

The force $d\vec{F}$ on the volume element dv at which the total current density is $\vec{J}$ is

$$d\vec{F} = \left(\vec{J} \times \vec{B}\right)dv \qquad (5a)$$

where the flux density vector $\vec{B}$ will be entirely on the x-y plane, because the current density vector has component only in the z-direction. Also, due to the symmetry, the direction of the force will be only in the x-direction. As a consequence, the force per unit length acting on finite element *e* of conductor *i* will be equal to

$$\vec{F}^e_i = \hat{x}\, F^e_{xi} \qquad (5b)$$

where the x-direction force per unit length of this element will be equal to

$$F^e_{xi} = -\iint_{S^e_i} J^e_z(x,y) B^e_y \, dxdy \qquad (6)$$

Because the flux density components in (6) are constant on the cross section of element *e*, the integral is easily expressed using symmetric quadrature formulae of first degree. If now the phasors related to the total element current I^e and to the flux density component B_y are

$$I^e = I^e_{rms}\, e^{j\,\theta^e}$$
$$B^e_y = B^e_{y\,rms}\, e^{j\,\varphi^e_y} \qquad (7)$$

the x-direction force per unit length time function in this element will be

$$f^e_x(t) = -I^e_{rms}\; B^e_{y\,rms}\left[\cos\left(\theta^e - \varphi^e_y\right) + \cos\left(2\omega t + \theta^e + \varphi^e_y\right)\right] \qquad (8)$$

and the total force time function, that defines the total force acting on conductor *i*, will be derived as the assembly of the elementary force contributions of this conductor

$$f_x(t) = \sum_e f^e_x(t) \qquad (9)$$

TABLE 1
RATED VALUES AND DIMENSIONS OF THE TWO TYPICAL BUSBAR ARRANGEMENTS

	U_N	I_{k3}	$\frac{i_{p3}}{\sqrt{2}}$	b	d	a	a_m
Arrangement	[V]	[kA]	[kA]	[m]	[m]	[m]	[m]
Low Voltage	380	17.55	28.08	0.080	0.010	0.160	0.1662
Medium Voltage	15,000	9.62	14.24	0.050	0.005	0.235	0.2367

leading to a total force per unit length vector

$$\bar{f}(t) = \hat{x} f_x(t) \tag{10}$$

It must be noted that the sum defined in (9) may be confined to a sub-conductor of a main conductor, if the integration is over this sub-conductor cross-section, or it may be extended to the main conductor of phase i, if the integration is over the total cross-section of the main conductor S_i. In every case, the locus of the force vector defined in (10) in the f_x-f_y plane and for a time variation equal to the half current period is a line segment with its centre located at

$$f_{xc} = -\sum_e I^e_{rms} B^e_{y\,rms} \cos\left(\theta^e - \varphi^e_y\right) \quad , \qquad f_{yc} = 0 \tag{11}$$

III. PARAMETRICAL ANALYSIS OF FORCES

Two typical busbar arrangements, one for low voltage and one for medium voltage indoor installations respectively, have been used as a reference for the calculation performed with the finite element procedure. The low voltage busbars are connected to a 630 kVA, 15 kV/380 V Dyn5 transformer with rated short-circuit voltage 6% and copper losses 6500 W. This results to I_{k3} = 17.55 kA and to R/X ratio equal to 0.175, leading through (1a) to κ = 1.6 and through (1b) to i_{p3} = 39.71 kA. The medium voltage busbars are connected to a typical 15 kV network with 250 MVA short-circuit capacity (fault level) and with R/X ratio equal to 0.25, so that I_{k3} = 9.62 kA, κ = 1.48 and i_{p3} = 20.14 kA. The rated and geometrical data of the two cases are shown in Table 1.

A. Calculations according to Standards

The maximum force per unit length F_{mb} acting on the central conductor (phase *b*) of Fig. 1a-b is given in [1]-[2] by

$$F_{mb} = \frac{\mu_0}{2\pi a} \frac{\sqrt{3}}{2} i^2_{p3} \tag{12a}$$

assuming that the dimensions of the busbar cross-sections are smaller than the distance a between the conductor centres, i.e. assuming the formula of filamentary conductors. Maximum force per unit length values F_{ma} and F_{mc} for the outer conductors (phases *a* and *c* respectively) are omitted in [1]-[2], because they are smaller than F_{mb}. However, they may be calculated according to [5] as follows:

$$F_{ma} = F_{mc} = \frac{\mu_0}{2\pi a} \frac{3+2\sqrt{3}}{8} i^2_{p3} \tag{12b}$$

The assumption of filamentary conductors on which (12a-b) are based, is corrected in the revisions [8]-[9]. Instead of the centre-line distance a, a new effective distance a_m has been introduced. This may be computed from Fig. 1 of [8] or alternatively from an equation given in Annex A of [8], in which a typographical error has been detected (factor 2 that multiplies the last arctan function in the last line should be omitted). On the last column of Table 1 of the present work, values of this effective distance a_m are shown for both arrangements. The maximum force per unit length F_{mb} acting on the central conductor (phase *b*) of Fig. 1a-b is now given in [8]-[9] as a function of a_m by

$$F_{mb} = \frac{\mu_0}{2\pi a_m} \frac{\sqrt{3}}{2} i^2_{p3} \tag{13a}$$

Maximum force per unit length values for the outer conductors, which for the same reason are omitted also in [8] and [9], may be written following again [5] and using the new effective distance a_m as

$$F_{ma} = F_{mc} = \frac{\mu_0}{2\pi a_m} \frac{3+2\sqrt{3}}{8} i^2_{p3} \tag{13b}$$

Finally, for multiple sub-conductors per mail conductor, a maximum force acting on the outer sub-conductors of phase *i* main conductor is given in [1], [2], [8] and [9] by

$$F_{mis} = \frac{\mu_0}{2\pi a_s} \left(\frac{i_{p3}}{n_s}\right)^2 \tag{14}$$

where a_s is the effective distance between sub-conductors.

It must be noted that this maximum force (although not clearly stated in [1], [2], [8] and [9]) is only the maximum of the force component that acts on the outer sub-conductor due to the current of phase *i* main conductor only. In order to compute the total force acting on an outer sub-conductor, the corresponding total force components (13a-b) must be divided by n_s and the result must be added or subtracted from the value given by (14). However, because there are no times attached to (13a-b) or to (14) and on the other hand the corresponding maxima arrive at different times, an exact calculation of the total maximum force using the Standards is impossible. In [1], [2], [8] and [9] this problem is eluded by:

- the limitation of the bending stress caused by forces between sub-conductors at $R_{p0,2}$;
- the limitation of the bending stress caused by forces between the main conductor and the sub-conductors at $q R_{p0,2}$.

It must be also noted that in (14) the effective distance a_s is introduced, in order to take into account the geometrical configuration and the profile of the arrangement of each main conductor. In [1], [2], [8] and [9] values of a_s are tabulated for the most common busbar profiles, while for other cases a relation for a_s is provided based on Lehmann calculations [3]. As stated in the Standards, (14) is valid only for the first and last sub-conductor, i.e. [1], [2], [8] and [9] do not supply force relations for the inner sub-conductors of every mail conductor. However, this is not required, since the maximum forces are those acting on the outer sub-conductors.

B. FEM Calculations - One sub-conductor per main conductor

The two busbar arrangements of Table 1, having originally one sub-conductor per main conductor, were solved with the FEM formulation of this paper and the maximum forces acting on the three conductors were compared with those

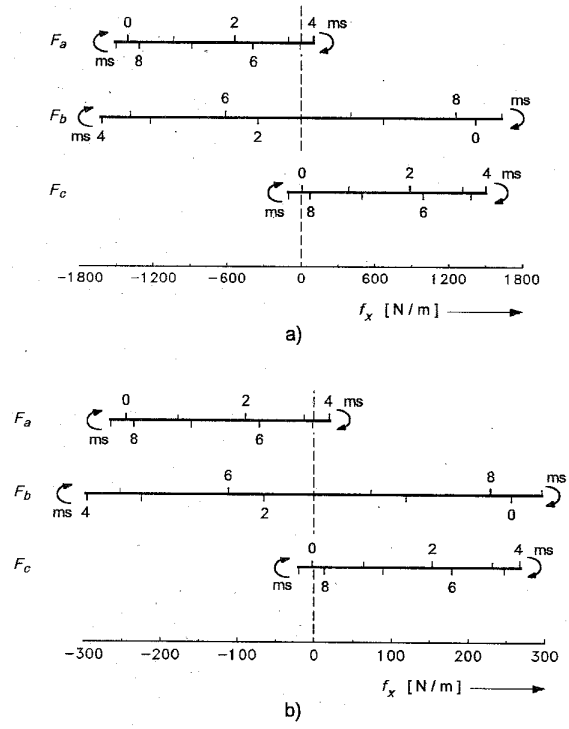

Fig. 2. Forces acting on the main conductors in the low and medium voltage arrangements of Table 1 for a time variation equal to a half period, with one sub-conductor per main conductor: a) low voltage and b) medium voltage arrangements.

given by (12a-b) and (13a-b). The forces acting on the main conductors and the resulting maximum force values are shown in Fig. 2 and Table 2 respectively. These results lead to the following conclusions:

- force maxima computed by (12a-b) seem to be on the safe side;
- force maxima computed by (13a-b) are also on the safe side but they approach better the maxima computed by FEM;
- force maxima computed by the FEM approach those computed by (12a-b) and (13a-b) as the cross-section of the busbars decreases and the distance between main conductors increases.

In order to clarify the last conclusion, the next two computations had as a parameter the busbar height b and the centre-line distance between main conductors a. The results concerning the low voltage arrangement are shown in Tables 3-4, where the parameters not explicitly defined are again taken from Table 1. In Table 3 the FEM maximum forces are shown to decrease strongly as the busbar height increases from $b/2$ to $8b$, since the increase of the busbar height leads to smaller current density values in the busbar cross-section and finally to smaller forces. The corresponding maximum force relations (12a-b), which are independent of b, lead to a constant value for all cases. On the other hand, the maximum force relations (13a-b), which are a function of b through their dependence on a_m, are shown to be almost equal to the corresponding FEM values. In Table 4 the differences between the FEM maximum forces and the corresponding values computed from (12a-b) and (13a-b) are shown to decrease as the distance between main conductors a increases, because in this case the assumptions in which (12a-b) and (13a-b) are based are better approximated. Values obtained from (13a-b) are again almost equal to the corresponding FEM maxima.

TABLE 2

	Low voltage arrangement					Medium voltage arrangement				
	FEM	(12a-b)	Difference	(13a-b)	Difference	FEM	(12a-b)	Difference	(13a-b)	Difference
	[N/m]	[N/m]	%	[N/m]	%	[N/m]	[N/m]	%	[N/m]	%
F_{ma}	1506.6	1592.8	-5.7	1533.1	-1.8	264.7	278.9	-5.4	276.8	-4.6
F_{mb}	1632.1	1707.1	-4.6	1643.2	-0.7	296.4	298.9	-0.8	296.7	-0.1
F_{mc}	1506.4	1592.8	-5.7	1533.1	-1.8	267.9	278.9	-4.1	276.8	-3.3

Maximum forces applied on the busbars of Table 1 calculated by FEM and compared to (12a-b) and (13a-b) respectively.

TABLE 3

	F_{ma}					F_{mb}				
b	FEM	(12b)	Difference	(13b)	Difference	FEM	(12a)	Difference	(13a)	Difference
[m]	[N/m]	[N/m]	%	[N/m]	%	[N/m]	[N/m]	%	[N/m]	%
0.04	1512.7	1592.8	-5.3	1577.6	-4.3	1724.4	1707.1	1.0	1690.8	1.9
0.16	1388.3	1592.8	-14.7	1398.4	-0.7	1447.8	1707.1	-17.9	1498.8	-3.5
0.32	1106.8	1592.8	-43.9	1122.8	-1.4	1134.9	1707.1	-50.4	1203.4	-6.0
0.64	782.3	1592.8	-103.6	773.9	1.1	785.5	1707.1	-117.3	829.4	-5.6

Finite element maximum force computation of the low voltage arrangement of Table 1, with varying busbar height b. The differences refer again to the force values given by (12a-b) and (13a-b).

TABLE 4

	a = 0.11 m					a = 0.21 m				
	FEM	(12a-b)	Difference	(13a-b)	Difference	FEM	(12a-b)	Difference	(13a-b)	Difference
	[N/m]	[N/m]	%	[N/m]	%	[N/m]	[N/m]	%	[N/m]	%
F_{ma}	2104.1	2316.8	-10.1	2148.6	-2.1	1161.0	1213.5	-4.5	1186.2	-2.2
F_{mb}	2252.0	2483.1	-10.3	2302.8	-2.3	1273.5	1300.7	-2.1	1271.3	0.2
F_{mc}	2058.5	2316.8	-12.5	2148.6	-4.4	1186.7	1213.5	-2.3	1186.2	0.0

Finite element maximum force computation of the low voltage arrangement of Table 1 with varying centre-line distance between main conductors a.

TABLE 5

	phase *a*		phase *b*		phase *c*	
	Force [N/m]	Current [kA]	Force [N/m]	Current [kA]	Force [N/m]	Current [kA]
	$n_s = 2$					
Sub-conductor 1 (FEM)	1175.4	$13.45\angle -9.1^o$	2288.4	$17.31\angle 229.1^o$	2651.2	$16.14\angle 121.8^o$
Sub-conductor 2 (FEM)	2635.6	$14.95\angle 8.1^o$	2039.7	$11.56\angle 256.5^o$	1203.5	$11.96\angle 117.6^o$
Main conductor (FEM)	1575.3	$28.08\angle 0.0^o$	1685.7	$28.08\angle 240.0^o$	1519.3	$28.08\angle 120.0^o$
Main conductor (12a-b)	1592.8	$28.08\angle 0.0^o$	1707.1	$28.08\angle 240.0^o$	1592.8	$28.08\angle 120.0^o$
Main conductor (13a-b)	1539.8	$28.08\angle 0.0^o$	1650.4	$28.08\angle 240.0^o$	1539.8	$28.08\angle 120.0^o$
	$n_s = 3$					
Sub-conductor 1 (FEM)	870.7	$9.05\angle -5.1^o$	2168.3	$14.09\angle 225.2^o$	2331.3	$13.91\angle 126.8^o$
Sub-conductor 2 (FEM)	192.3	$7.28\angle -27.6^o$	300.2	$7.13\angle 212.1^o$	116.6	$7.00\angle 93.0^o$
Sub-conductor 3 (FEM)	2288.5	$13.29\angle 18.3^o$	1723.1	$10.71\angle 280.4^o$	811.0	$8.18\angle 130.7^o$
Main conductor (FEM)	1665.6	$28.08\angle 0.0^o$	1761.4	$28.08\angle 240.0^o$	1588.1	$28.08\angle 120.0^o$
Main conductor (12a-b)	1592.8	$28.08\angle 0.0^o$	1707.1	$28.08\angle 240.0^o$	1592.8	$28.08\angle 120.0^o$
Main conductor (13a-b)	1553.6	$28.08\angle 0.0^o$	1665.2	$28.08\angle 240.0^o$	1553.6	$28.08\angle 120.0^o$
	$n_s = 4$					
Sub-conductor 1 (FEM)	609.1	$7.49\angle -2.8^o$	2111.9	$13.33\angle 222.8^o$	2197.4	$13.48\angle 128.7^o$
Sub-conductor 2 (FEM)	45.6	$4.11\angle -35.7^o$	118.1	$5.18\angle 192.8^o$	191.1	$5.27\angle 90.8^o$
Sub-conductor 3 (FEM)	245.9	$5.54\angle -23.4^o$	240.3	$4.59\angle 231.6^o$	69.4	$3.73\angle 96.3^o$
Sub-conductor 4 (FEM)	2191.5	$13.15\angle 22.2^o$	1672.8	$11.13\angle 289.1^o$	559.3	$7.04\angle 136.9^o$
Main conductor (FEM)	1811.2	$28.08\angle 0.0^o$	1903.1	$28.08\angle 240.0^o$	1706.8	$28.08\angle 120.0^o$
Main conductor (12a-b)	1592.8	$28.08\angle 0.0^o$	1707.1	$28.08\angle 240.0^o$	1592.8	$28.08\angle 120.0^o$
Main conductor (13a-b)	1575.3	$28.08\angle 0.0^o$	1688.4	$28.08\angle 240.0^o$	1575.3	$28.08\angle 120.0^o$

Finite element computation of maximum forces and of rms current distribution in the low voltage arrangement described in Table 1 with 2, 3 and 4 sub-conductors per main conductor. The maximum forces acting on the main conductors and obtained from (12a-b) and (13a-b) for the three cases respectively are also shown.

TABLE 6

	phase *a*		phase *b*		phase *c*	
	Force [N/m]	Current [kA]	Force [N/m]	Current [kA]	Force [N/m]	Current [kA]
	$n_s = 2$					
Sub-conductor 1 (FEM)	718.7	$7.16\angle -1.35^o$	885.5	$7.46\angle 239.3^o$	976.4	$7.25\angle 121.0^o$
Sub-conductor 2 (FEM)	956.5	$7.07\angle 1.37^o$	846.8	$6.78\angle 240.8^o$	713.6	$6.99\angle 119.0^o$
Main conductor (FEM)	271.3	$14.24\angle 0.0^o$	307.8	$14.24\angle 240.0^o$	278.8	$14.24\angle 120.0^o$
Main conductor (12a-b)	278.9	$14.24\angle 0.0^o$	298.9	$14.24\angle 240.0^o$	278.9	$14.24\angle 120.0^o$
Main conductor (13a-b)	277.0	$14.24\angle 0.0^o$	296.9	$14.24\angle 240.0^o$	277.0	$14.24\angle 120.0^o$
	$n_s = 3$					
Sub-conductor 1 (FEM)	577.7	$4.86\angle 0.9^o$	727.5	$5.41\angle 240.8^o$	770.5	$5.15\angle 126.1^o$
Sub-conductor 2 (FEM)	80.1	$4.62\angle -9.6^o$	113.2	$4.62\angle 230.4^o$	67.1	$4.61\angle 110.4^o$
Sub-conductor 3 (FEM)	739.0	$4.87\angle 8.2^o$	624.8	$4.33\angle 249.2^o$	554.2	$4.58\angle 122.7^o$
Main conductor (FEM)	265.0	$14.24\angle 0.0^o$	302.4	$14.24\angle 240.0^o$	274.9	$14.24\angle 120.0^o$
Main conductor (12a-b)	278.9	$14.24\angle 0.0^o$	298.9	$14.24\angle 240.0^o$	278.9	$14.24\angle 120.0^o$
Main conductor (13a-b)	277.3	$14.24\angle 0.0^o$	297.2	$14.24\angle 240.0^o$	277.3	$14.24\angle 120.0^o$
	$n_s = 4$					
Sub-conductor 1 (FEM)	433.7	$3.77\angle 4.5^o$	601.8	$4.50\angle 242.6^o$	627.1	$4.31\angle 131.8^o$
Sub-conductor 2 (FEM)	87.6	$3.36\angle -14.6^o$	127.8	$3.59\angle 224.9^o$	179.9	$3.49\angle 108.5^o$
Sub-conductor 3 (FEM)	194.9	$3.40\angle -10.0^o$	187.8	$3.16\angle 230.7^o$	109.6	$3.24\angle 106.8^o$
Sub-conductor 4 (FEM)	591.1	$4.05\angle 16.4^o$	469.2	$3.40\angle 261.6^o$	408.6	$3.49\angle 129.3^o$
Main conductor (FEM)	281.5	$14.24\angle 0.0^o$	307.1	$14.24\angle 240.0^o$	279.4	$14.24\angle 120.0^o$
Main conductor (12a-b)	278.9	$14.24\angle 0.0^o$	298.9	$14.24\angle 240.0^o$	278.9	$14.24\angle 120.0^o$
Main conductor (13a-b)	277.8	$14.24\angle 0.0^o$	297.8	$14.24\angle 240.0^o$	277.8	$14.24\angle 120.0^o$

Finite element computation of maximum forces and of rms current distribution in the medium voltage arrangement described in Table 1 with 2, 3 and 4 sub-conductors per main conductor. The maximum forces acting on the main conductors and obtained from (12a-b) and (13a-b) for the three cases respectively are also shown.

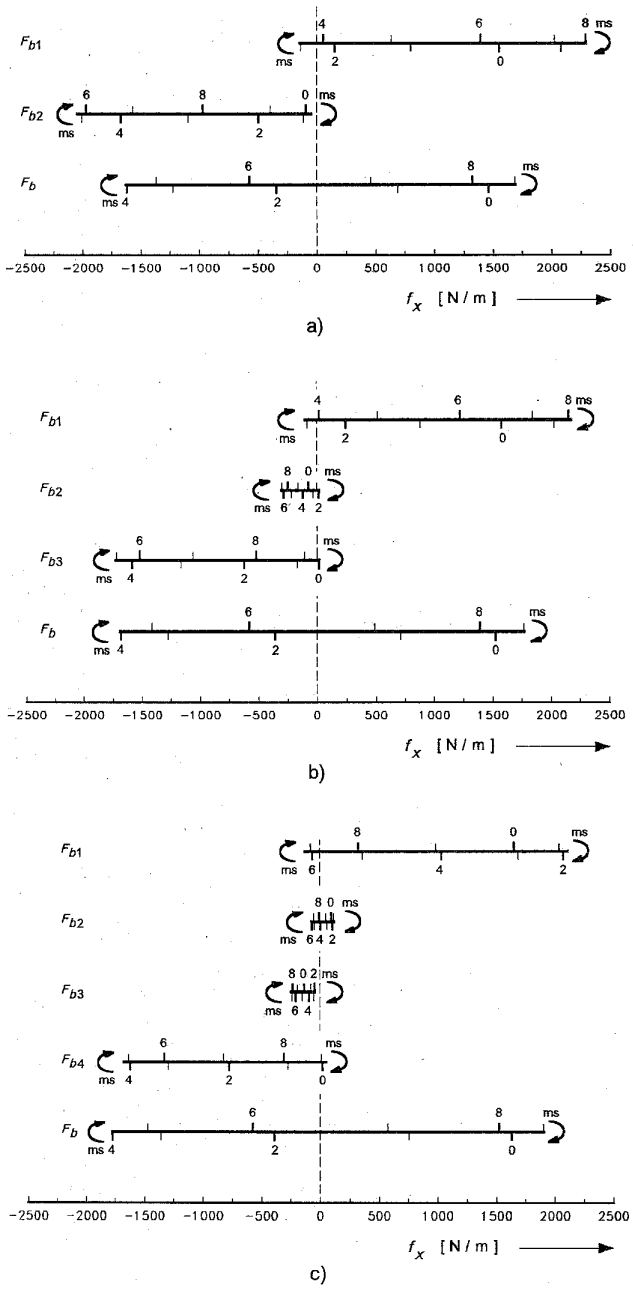

Fig. 3. Forces acting on the middle main conductor in the low voltage arrangement with a) two, b) three and c) four sub-conductors per main conductor.

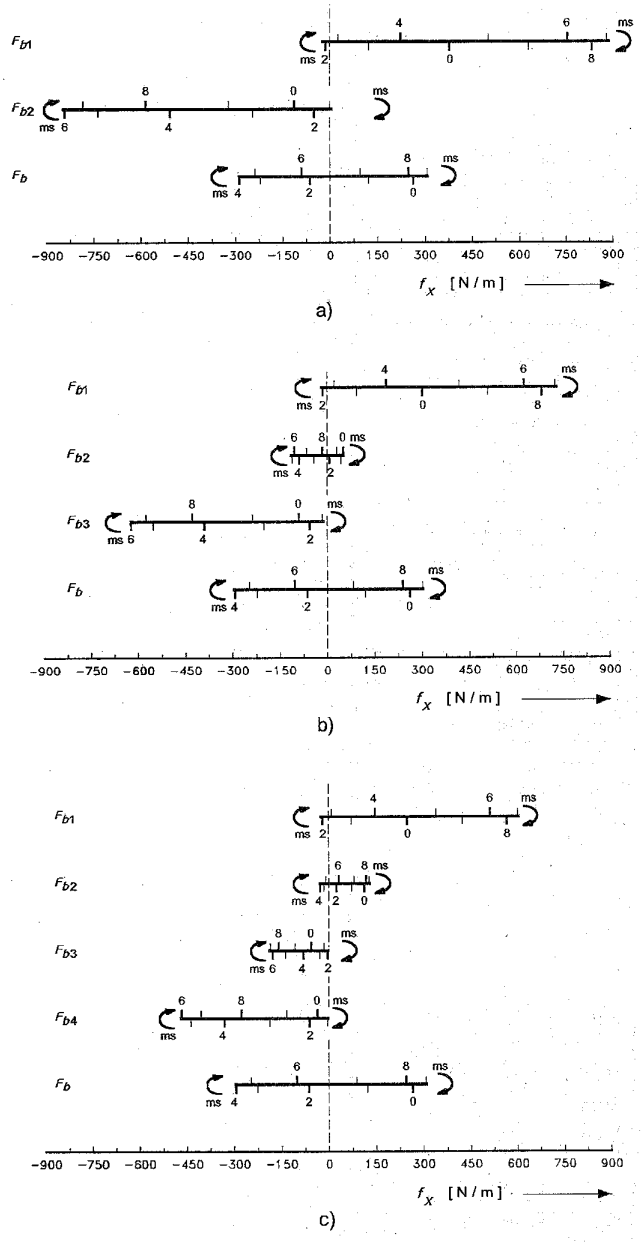

Fig. 4. Forces acting on the middle main conductor in the medium voltage arrangement with a) two, b) three and c) four sub-conductors per main conductor.

C. FEM Calculations - Multiple sub-conductors per main conductor

The next computation concerns arrangements with more than one sub-conductor per main conductor. With their geometry shown in Fig. 1 and described in Table 1, three cases with n_s = 2, 3 and 4 sub-conductors in every main conductor respectively are solved with the FEM. The results are shown in Fig. 3 and in Table 5 for the low voltage and in Fig. 4 and in Table 6 for the medium voltage arrangement respectively. A comparison with the corresponding partial force values obtained from (14) for the outer sub-conductors cannot be made, for the reason explained above. Anyway, the comparison with the corresponding main conductor maximum forces obtained from (12a-b) and (13a-b), as well as the current distribution among the sub-conductors of every main conductor shown in Tables 5-6, lead to the following conclusions:

- maximum forces computed according to (12a-b), which are independent of n_s, are in many cases smaller than those computed by the FEM solution, i.e. [1] and [2] are not always on the safe side;
- maximum forces computed according to (13a-b), which are a function of n_s (because as stated in [8] and [9], the effective distance a_m may be computed in this case by setting $d = d_m$), are still in some cases smaller than those computed by the FEM solution;
- the low voltage arrangement, due to the smaller dis-

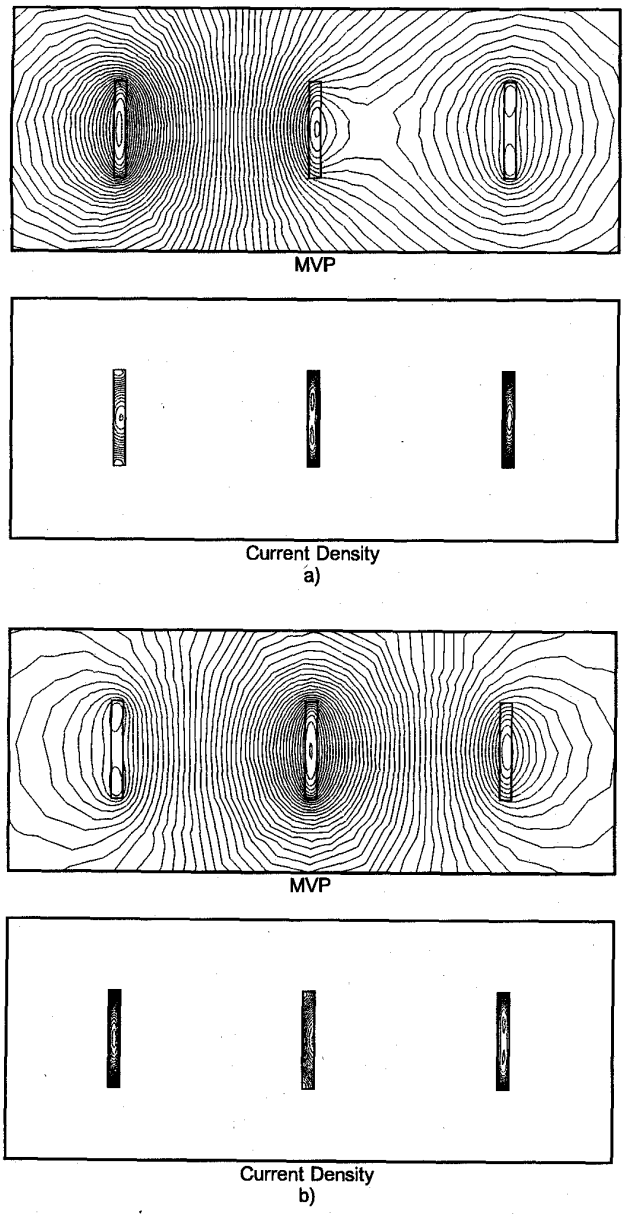

Fig. 5. Magnetic vector potential and total current density distribution in the low voltage arrangement with one sub-conductor per main conductor: a) at $\omega t = 0°$ and b) at $\omega t = 120°$.

tance between main conductors and to the larger conductor profile, leads to considerably stronger deviations from [1], [2], [8] and [9] as compared with the medium voltage arrangement;

- the assumption of [3] that the n_s sub-conductors of phase i main conductor carry the short-circuit current evenly distributed among them cannot be justified (the rms value of the current flowing in every sub-conductor as well as its corresponding phase angles present significant differences).

Finally, in Fig. 5a-b the lines of constant A_z and of constant J_z for the arrangement of Fig. 1a are plotted when the short-circuit current is at its maximum in phase a ($\omega t = 0°$) and in phase b ($\omega t = 0°$) main conductors respectively, and in Fig. 6a-b for the arrangement shown Fig. 1b. In both Figures the lines of MVP differ by $0.5 \cdot 10^{-3}$ Wb/m, while those of current density differ by $2 \cdot 10^6$ A/m^2. The lines of constant A_z in a two-dimensional problem are the lines of magnetic flux, so the distribution of the field in the cross-section of the busbar may be estimated from Fig. 5a and Fig. 6a. The symmetry of the magnetic field justifies the fact that the forces are always on the x-direction. On the other side, the distribution of the current density as obtained from the FEM solution takes into account both the skin and proximity effects. From the current density lines shown in Fig. 5b and Fig. 6b is concluded that the current is strongly influenced by the busbar geometry and in every case unevenly distributed in the sub-conductors of every main conductor.

IV. Conclusions

The Finite Element Method (FEM) calculation of field and forces for three-phase rigid busbars presented in this paper leads to significant differences as compared with IEC and DIN/VDE Standards [1]-[2]. Moreover, the assumption of [1]-[2] that the partial currents in sub-conductors of each main conductor are equal cannot be justified, as FEM leads to differences up to 1:3. Although in the revisions [8]-[9] of the Standards the introduction of an *effective distance* between the main conductors leads to maximum force values almost equal to the FEM solution in arrangements with one sub-conductor per main conductor, this does not always happen when the arrangement has two or more sub-conductors per main conductor. The results suggest that a further consideration of [8]-[9] may be useful, especially in cases with multiple sub-conductors per main conductor.

V. List of Symbols

A : magnetic vector potential (MVP) (Wb/m)
a : centre-line distance between main conductors (Fig. 1) (m)
a_m : effective distance between main conductors (defined in 2.2.1.4 of [8]) (m)
a_s : effective distance between sub-conductors (Table 1 of [1] and [2]) (m)
B : flux density (T)
b : sub-conductor dimension perpendicular to the force direction (Fig. 1) (m)
b_m : main conductor dimension perpendicular to the force direction (Fig. 1) (m)
d : sub-conductor dimension in the force direction (Fig. 1) (m)
d_m : main conductor dimension in the force direction (Fig. 1) (m)
e : finite element (superscript)
F_i : total force per unit length acting on phase i main conductor during a balanced three-phase short-circuit (N/m)
F_{is} : total force per unit length acting on sub-conductor s of phase i main conductor during a balanced three-phase short-circuit (N/m)
F_{mi} : maximum total force per unit length acting on phase i main conductor during a balanced three-phase short-circuit (N/m)
F_{mis} : maximum force per unit length of the force component that acts on sub-conductor s of phase i main conductor and is due to current of this main conductor only, during a balanced three-phase short-circuit (N/m)
f_x, f_y : x- and y-direction components of the force per unit length (N/m)

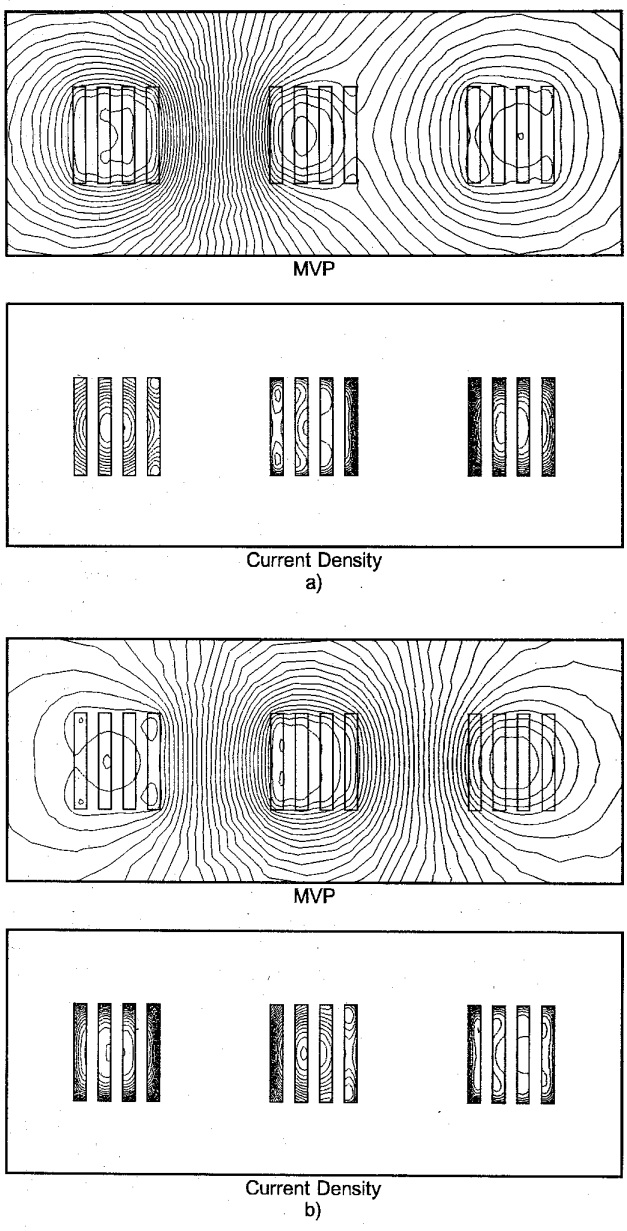

Fig. 6. Magnetic vector potential and total current density distribution in the low voltage arrangement with four sub-conductors per main conductor: a) at $\omega t = 0°$ and b) at $\omega t = 120°$.

f	: frequency	(Hz)
i	: phase sequence index (i = a, b, c)	
I_{k3}	: rms three-phase symmetrical short-circuit current	(kA)
i_{p3}	: peak short-circuit current in case of a balanced three-phase short-circuit	(kA)
J	: total current density	(A/m^2)
J_e	: eddy current density	(A/m^2)
J_s	: source current density	(A/m^2)
n_s	: number of sub-conductors per main conductor	
q	: factor of plasticity	
R	: resistance	(Ω)
$R_{p0,2}$	: stress corresponding to the yield point	(N/m^2)
rms	: root mean square (subscript)	
S_i	: total cross-section of n_s sub-conductors of phase i main conductor	(m^2)
s	: sub-conductor index (s = 1, 2, 3, . . ., n_s)	
t	: time	(s)
U_N	: nominal line-to-line voltage (rms)	(V)
X	: reactance	(Ω)
θ	: current phase angle	(rad)
κ	: factor for peak current	
μ_r	: relative permeability of conductor material	
μ_0	: relative permeability of vacuum	(400π nH/m)
φ	: flux density phase angle	(rad)
ω	: circular frequency	(s^{-1})

VI. Acknowledgements

The authors gratefully acknowledge the contribution of Mr. G. Mantos and Mr. D. Pallas, graduate students of Dept. of Electrical and Computer Engineering of the Aristotle University of Thessaloniki, who prepared and computed several cases of this paper.

VII. References

[1] IEC-Publ. 865/1986, "Calculation of the effects of short-circuit currents," Geneve/Suisse: Bureau Central de la CEI.

[2] DIN/VDE 0103, 04/88, "Bemessung von Starkstromanlagen auf mechanische und thermische Kurzschlußfestigkeit," Berlin/Germany: VDE-VERLAG.

[3] W. Lehmann, "Elektrodynamische Beanspruchung paralleler Leiter," *ETZ-A*, Bd. 76, 1955, pp. 481-488.

[4] J. Weiss and Z. Csendes, "A one-step finite element method for multiconductor skin effect problems," *IEEE Transactions on Power Apparatus and Systems*, vol. PAS-101, October 1982, pp. 3796-3803.

[5] G. Hosemann and D. Tsanakas, "Dynamic short-circuit stress of busbar structures with stiff conductors. Parametric studies and conclusions for simplified calculation methods," *Electra*, no.68, 1980, pp. 37-64.

[6] IEC TC 73, 07/84: Short-circuit currents, Working group 01. Calculation of currents. IWD Section I: Systems supplied through transformers.

[7] D. Labridis and P. Dokopoulos, "Finite element computation of field, losses and forces in a three-phase gas cable with non-symmetrical conductor arrangement," *IEEE Transactions on Power Delivery*, vol. PWDR-3, October 1988, pp. 1326-1333.

[8] IEC-Publ. 865/1993: Short-circuit currents - Calculation of effects. Part 1: Definitions and calculation methods. Geneve/Suisse: Bureau Central de la CEI.

[9] Entwurf DIN/VDE 0103, 06/92: Berechnung der Wirkung von Kurzschlußströmen. Berlin/Germany: VDE-VERLAG.

VIII. Biographies

Dimitris Labridis (S' 88-M' 90) was born in Thessaloniki, Greece, on July 26, 1958. He received the Dipl.-Eng. degree and the Ph.D. degree from the Department of Electrical Engineering at the Aristotle University of Thessaloniki, in 1981 and 1989 respectively.

During 1982-1993 he has been working, at first as a research assistant and later as a Lecturer, at the Department of Electrical Engineering at the Aristotle University of Thessaloniki, Greece. Since 1994 he has been an Assistant Professor at the same Department. His special interests are power system analysis with special emphasis on the simulation of transmission and distribution systems, electromagnetic and thermal field analysis and numerical methods in engineering.

Petros Dokopoulos (M' 77) was born in Athens, Greece, in September 1939. He received the Dipl. Eng. degree from the Technical University of Athens in 1962 and the PhD degree from the University of Brunswick, Germany, in 1967.

During 1962-1967 he was with the Laboratory for High Voltage and Transmission at the University of Brunswick, Germany, during 1967-1974 with the Nuclear Research Centre at Julich, Germany, and during 1974-1978 with the Joint European Torus. Since 1978 he has been full professor at the Department of Electrical Engineering at the Aristotle University of Thessaloniki, Greece. He has worked as consultant to Brown Boveri and Cie, Mannheim, Germany, to Siemens, Erlagen, Germany, to Public Power Corporation, Greece and to National Telecommunication Organisation, Greece. His scientific fields of interest are dielectric's, power switches, generators, power cables, alternative energy sources, transmission and distribution and fusion. He has 65 publications and 7 patents on these subjects.